High-precision three-dimensional Rydberg atom localization in a four-level atomic system*

Hengfei Zhang(张恒飞)[1,2], Jinpeng Yuan(元晋鹏)[1,2,†], Lirong Wang(汪丽蓉)[1,2,‡], Liantuan Xiao(肖连团)[1,2], and Suo-tang Jia(贾锁堂)[1,2]

[1] State Key Laboratory of Quantum Optics and Quantum Optics Devices, Institute of Laser Spectroscopy, Shanxi University, Taiyuan 030006, China

[2] Collaborative Innovation Center of Extreme Optics, Shanxi University, Taiyuan 030006, China

(Received 17 November 2020; revised manuscript received 11 December 2020; accepted manuscript online 17 December 2020)

Rydberg atoms have been widely investigated due to their large size, long radiative lifetime, huge polarizability and strong dipole-dipole interactions. The position information of Rydberg atoms provides more possibilities for quantum optics research, which can be obtained under the localization method. We study the behavior of three-dimensional (3D) Rydberg atom localization in a four-level configuration with the measurement of the spatial optical absorption. The atomic localization precision depends strongly on the detuning and Rabi frequency of the involved laser fields. A 100% probability of finding the Rydberg atom at a specific 3D position is achieved with precision of $\sim 0.031\lambda$. This work demonstrates the possibility for achieving the 3D atom localization of the Rydberg atom in the experiment.

Keywords: Rydberg atom, three-dimensional localization, standing-wave field

PACS: 32.80.Qk, 32.80.Rm, 42.50.Gy, 42.50.Nn **DOI:** 10.1088/1674-1056/abd46f

1. Introduction

Rydberg atoms are high-excited atoms with large principal quantum numbers, which have attracted considerable focus recently for the demonstrated remarkable properties.[1] The large size and long radiative lifetime make the Rydberg quantum system have a long coherence time.[2] The Rydberg atom is sensitive to external electric field since the huge polarizability.[3] In addition, the strong long-range dipole–dipole interactions lead to the investigation of dipole blockade effects.[4] Based on these peculiar properties, Rydberg atoms are greatly applied in ultra-cold plasmas,[5] many-body physics,[6] quantum information,[7] quantum computing,[8] and microwave field measurements.[9]

In the applications based on Rydberg atoms, the research of localization provides the position information of the Rydberg atom in spatial coordinates. Over the past few decades, the high-precision atom localization has been used in trapping and cooling of atoms,[10] atom nanolithography,[11,12] coherent patterning of matter waves[13] and Bose–Einstein condensation.[14] The proposal to use quantum interference and atomic coherence effect has already been applied for atom localization in one-dimensional (1D)[15,16] and two-dimensional (2D) space.[17,18] Until recent years, research interest transfers to three-dimensional (3D) space. Several high-precision 3D atom localization schemes have been proposed by measuring the probe absorption, spontaneous emission, and Kerr nonlinearity.[19–24]

Even though there are many efficient schemes for atom localization, until now only a few Rydberg atom localization have been reported.[25] The large size of the Rydberg atom makes it a good candidate for studying the quantum coherence phenomena. For achieving the high-precision localization of a Rydberg atom, an effective scheme is needed. Recently, an experiment realization of the Rydberg atom based on a four-level atomic system in Ref. [26] attracts our attention. This system utilizes Rydberg level as the uppermost level and composed of two V- and Ξ-type electromagnetically induced transparency (EIT) systems, provides a novel configuration for studying the localization of Rydberg atom. Compared with the V- and Ξ-type atomic system of atom localization schemes, this four-level configuration increases the controllability of the experiment and produces more fantastic results.

In this work, a four-level atomic system is employed for realizing the high-precision 3D Rydberg atom localization. Three pairs of orthogonal standing-wave fields aligned respectively in the x, y, and z directions couple the same energy level transition of the Rydberg atom. Due to the interaction between the atom and fields, the 3D localization of a Rydberg atom is achieved by measuring the absorption of probe field, which is much more convenient to realize in experiment. In result, the maximum probability of finding the Rydberg atom is achieved as 100% in the sub-wavelength region. This scheme

*Project supported by the National R&D Program of China (Grant No. 2017YFA0304203), the National Natural Science Foundation of China (Grant Nos. 61875112, 61705122, 62075121, and 91736209), the Program for Sanjin Scholars of Shanxi Province, the Key Research and Development Program of Shanxi Province for International Cooperation (Grant No. 201803D421034), Shanxi Scholarship Council of China (Grant Nos. 2020-073), and 1331KSC.

†Corresponding author. E-mail: yjp@sxu.edu.cn

‡Corresponding author. E-mail: wlr@sxu.edu.cn

provides an effective way to realize the high-precision 3D Rydberg atom localization in the experiment.

2. Theoretical model

Taking cold ^{85}Rb atoms for the experimental implementation, a four-level atomic system involving a Rydberg state is considered as shown in Fig. 1, where level $|g\rangle$ is the ground state of $5S_{1/2}$, levels $|e\rangle$ and $|s\rangle$ denote the excited states of $5P_{3/2}$ and $5P_{1/2}$ and the level $|r\rangle$ is the $44D_{5/2}$ Rydberg state. The decay rates of these states are $\Gamma_g = 0$ MHz, $\Gamma_e = 2\pi \times 6.1$ MHz, $\Gamma_s = 2\pi \times 5.9$ MHz and $\Gamma_r = 2\pi \times 0.3$ MHz, respectively.[27] A weak probe field with Rabi-frequency Ω_p drives the $|g\rangle \to |e\rangle$ transition. The strong switching and control fields with Rabi frequencies Ω_s and Ω_c act on the transitions of $|g\rangle \to |s\rangle$ and $|e\rangle \to |r\rangle$, respectively. All three laser fields move along the z direction. Here, we employ three orthogonal standing-wave fields to couple the same transition of $|g\rangle \to |s\rangle$, i.e.,

$$\Omega = \Omega_x \sin(kx) + \Omega_y \sin(ky) + \Omega_z \sin(kz) + \Omega_s, \tag{1}$$

where k is the corresponding laser field wave vector, Ω_x, Ω_y and Ω_z are the Rabi frequencies of standing-wave fields propagating along x, y and z directions, respectively. We assume that the atom moves along the z direction, and passes through the intersecting region of the three orthogonal standing-wave fields in 3D space. As a consequence, the interaction between the atom and standing-wave fields is spatially dependent in the 3D space.

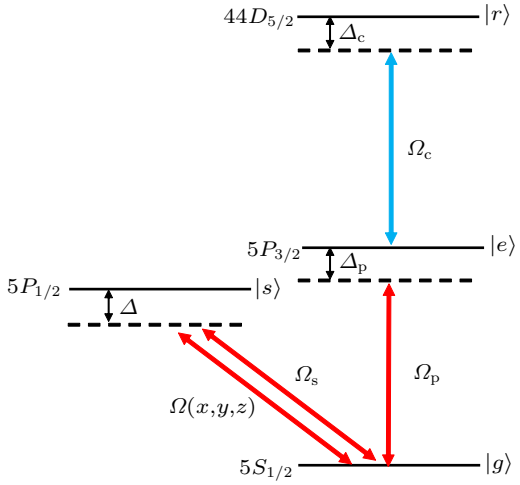

Fig. 1. Schematic diagram of a four-level ^{85}Rb atomic system. This system composes of two EIT configurations of V- and Ξ-type, which share the same probe field. The level $|g\rangle$ is the $5S_{1/2}$ ground state, levels $|e\rangle$ and $|s\rangle$ are the $5P_{3/2}$ and $5P_{1/2}$ excited states and the level $|r\rangle$ is the $44D_{5/2}$ Rydberg state.

Applying the rotating-wave and electric dipole approximation, the interaction picture Hamiltonian for this system is given by ($\hbar = 1$)

$$H_{\rm int} = \frac{1}{2}[\Omega_p|g\rangle\langle e| + \Omega|g\rangle\langle s| + \Omega_c|e\rangle\langle r|] + \Delta_p|e\rangle\langle e| + \Delta|s\rangle\langle s| + (\Delta_p + \Delta_c)|r\rangle\langle r| + \text{H.c.}, \tag{2}$$

where H.c. represents the Hermitian conjugation, and Δ_p, Δ, Δ_c denote the corresponding laser frequency detunings.

The observable in this scheme is the response of the atoms to applied laser fields, which is described by susceptibility of the weak probe field. The susceptibility is determined by the coherence between levels $|g\rangle$ and $|e\rangle$ and can be written as

$$\chi = \frac{N|\mu_{eg}|^2}{\varepsilon_0 \hbar \Omega_p} \rho_{eg}, \tag{3}$$

where N is the atomic density, ε_0 is the permittivity of free space, μ_{eg} and ρ_{eg} are the dipole momentum and density matrix element, respectively. According to Eq. (3), the density matrix element ρ_{eg} needs to be calculated for tracing the atomic response of the system to external fields. The dynamics of the system by the density matrix formalism are described as[28]

$$\frac{\partial \rho}{\partial t} = -\frac{\mathrm{i}}{\hbar}[H_{\rm int}, \rho] + L[\rho(t)], \tag{4}$$

where the Lindblad form of Liouvillian matrix $L[\rho(t)]$ describing the relaxation by spontaneous decay is expressed as

$$L[\rho(t)] = \begin{bmatrix} \Gamma_e\rho_{ee} + \Gamma_s\rho_{ss} & -\frac{\Gamma_e}{2}\rho_{ge} & -\frac{\Gamma_s}{2}\rho_{gs} & -\frac{\Gamma_r}{2}\rho_{gr} \\ -\frac{\Gamma_e}{2}\rho_{eg} & -\Gamma_e\rho_{ee} + \Gamma_r\rho_{rr} & -\frac{\Gamma_e+\Gamma_s}{2}\rho_{es} & -\frac{\Gamma_e+\Gamma_r}{2}\rho_{er} \\ -\frac{\Gamma_s}{2}\rho_{sg} & -\frac{\Gamma_s+\Gamma_e}{2}\rho_{se} & -\Gamma_s\rho_{ss} & -\frac{\Gamma_s+\Gamma_r}{2}\rho_{sr} \\ -\frac{\Gamma_r}{2}\rho_{rg} & -\frac{\Gamma_r+\Gamma_e}{2}\rho_{re} & -\frac{\Gamma_r+\Gamma_s}{2}\rho_{rs} & -\Gamma_r\rho_{rr} \end{bmatrix}. \tag{5}$$

Thus, the motion equations for the density-matrix elements are given by

$$\begin{aligned}
\frac{\partial \rho_{gg}}{\partial t} &= \Gamma_e\rho_{ee} + \Gamma_s\rho_{ss} + \frac{\mathrm{i}}{2}\Omega_p(\rho_{eg} - \rho_{ge}) + \frac{\mathrm{i}}{2}\Omega(\rho_{sg} - \rho_{gs}), \\
\frac{\partial \rho_{ee}}{\partial t} &= -\Gamma_e\rho_{ee} + \Gamma_r\rho_{rr} + \frac{\mathrm{i}}{2}\Omega_p(\rho_{ge} - \rho_{eg}) + \frac{\mathrm{i}}{2}\Omega_c(\rho_{re} - \rho_{er}), \\
\frac{\partial \rho_{ss}}{\partial t} &= -\Gamma_s\rho_{ss} + \frac{\mathrm{i}}{2}\Omega(\rho_{gs} - \rho_{sg}), \\
\frac{\partial \rho_{rr}}{\partial t} &= -\Gamma_r\rho_{rr} + \frac{\mathrm{i}}{2}\Omega_c(\rho_{er} - \rho_{re}), \\
\frac{\partial \rho_{eg}}{\partial t} &= \left(-\frac{\Gamma_e}{2} + \mathrm{i}\Delta_p\right)\rho_{eg} - \frac{\mathrm{i}}{2}\Omega_p(\rho_{ee} - \rho_{gg}) \\
&\quad - \frac{\mathrm{i}}{2}\Omega\rho_{es} + \frac{\mathrm{i}}{2}\Omega_c\rho_{rg}, \\
\frac{\partial \rho_{sg}}{\partial t} &= \left(-\frac{\Gamma_s}{2} + \mathrm{i}\Delta\right)\rho_{sg} - \frac{\mathrm{i}}{2}\Omega(\rho_{ss} - \rho_{gg}) - \frac{\mathrm{i}}{2}\Omega_p\rho_{se}, \\
\frac{\partial \rho_{rg}}{\partial t} &= \left[-\frac{\Gamma_r}{2} + \mathrm{i}(\Delta_p + \Delta_c)\right]\rho_{rg} + \frac{\mathrm{i}}{2}\Omega_c\rho_{eg} \\
&\quad - \frac{\mathrm{i}}{2}\Omega_p\rho_{re} - \frac{\mathrm{i}}{2}\Omega\rho_{rs}, \\
\frac{\partial \rho_{se}}{\partial t} &= \left[-\frac{\Gamma_s + \Gamma_e}{2} + \mathrm{i}(\Delta - \Delta_p)\right]\rho_{se} + \frac{\mathrm{i}}{2}\Omega\rho_{ge}
\end{aligned}$$

$$
\begin{aligned}
&-\frac{\mathrm{i}}{2}\Omega_{\mathrm{p}}\rho_{\mathrm{sg}}-\frac{\mathrm{i}}{2}\Omega_{\mathrm{c}}\rho_{\mathrm{sr}},\\
\frac{\partial\rho_{\mathrm{re}}}{\partial t} &= \left(-\frac{\Gamma_{\mathrm{r}}+\Gamma_{\mathrm{e}}}{2}+\mathrm{i}\Delta_{\mathrm{c}}\right)\rho_{\mathrm{re}}-\frac{\mathrm{i}}{2}\Omega_{\mathrm{c}}(\rho_{\mathrm{rr}}-\rho_{\mathrm{ee}})-\frac{\mathrm{i}}{2}\Omega_{\mathrm{p}}\rho_{\mathrm{rg}},\\
\frac{\partial\rho_{\mathrm{rs}}}{\partial t} &= \left[-\frac{\Gamma_{\mathrm{r}}+\Gamma_{\mathrm{s}}}{2}+\mathrm{i}(\Delta_{\mathrm{c}}+\Delta_{\mathrm{p}}-\Delta)\right]\rho_{\mathrm{rs}}\\
&\quad+\frac{\mathrm{i}}{2}\Omega_{\mathrm{c}}\rho_{\mathrm{es}}-\frac{\mathrm{i}}{2}\Omega\rho_{\mathrm{rg}}. \qquad (6)
\end{aligned}
$$

Therefore, under the weak probe field approximation, the steady-state solution for ρ_{eg} is given by

$$\rho_{\mathrm{eg}}=\frac{\mathrm{i}}{A}\Omega_{\mathrm{p}}\times(\gamma_{\mathrm{se}}\Omega^2+\gamma_{\mathrm{rg}}\Omega_{\mathrm{c}}^2+4\gamma_{\mathrm{se}}\gamma_{\mathrm{rg}}\gamma_{\mathrm{rs}}), \qquad (7)$$

where

$$
\begin{aligned}
A &= \Omega^2\Omega_{\mathrm{c}}^2-\Omega^4-\Omega_{\mathrm{c}}^4-2\Omega^2(\gamma_{\mathrm{eg}}\gamma_{\mathrm{se}}+\gamma_{\mathrm{rg}}\gamma_{\mathrm{rs}})\\
&\quad-3\Omega_{\mathrm{c}}^2(\gamma_{\mathrm{eg}}\gamma_{\mathrm{rg}}+\gamma_{\mathrm{se}}\gamma_{\mathrm{rs}})-8\gamma_{\mathrm{eg}}\gamma_{\mathrm{se}}\gamma_{\mathrm{rg}}\gamma_{\mathrm{rs}},
\end{aligned}
$$

and

$$
\begin{aligned}
&\gamma_{\mathrm{eg}}=-\frac{\Gamma_{\mathrm{e}}}{2}+\mathrm{i}\Delta_{\mathrm{p}},\quad \gamma_{\mathrm{rg}}=-\frac{\Gamma_{\mathrm{r}}}{2}+\mathrm{i}(\Delta_{\mathrm{p}}+\Delta_{\mathrm{c}}),\\
&\gamma_{\mathrm{se}}=-\frac{\Gamma_{\mathrm{s}}+\Gamma_{\mathrm{e}}}{2}+\mathrm{i}(\Delta-\Delta_{\mathrm{p}}),\\
&\gamma_{\mathrm{rs}}=-\frac{\Gamma_{\mathrm{r}}+\Gamma_{\mathrm{s}}}{2}+\mathrm{i}(\Delta_{\mathrm{c}}+\Delta_{\mathrm{p}}-\Delta).
\end{aligned}
$$

The imaginary part of the susceptibility can be used to express the absorption of the probe laser field, which reflects the atomic position distribution probability in 3D space when the atom interacts with the three standing-wave fields. Probe absorption can localize the atom at a particular position in sub-wavelength space under the proper parameters. Therefore, the 3D atom position information can be obtained with the measurement of probe absorption $\mathrm{Im}(\chi)$.

3. Results and discussion

The probe absorption versus positions (kx,ky,kz) for different probe field frequency detunings Δ_{p} is plotted in Fig. 2, where $\Delta=\Delta_{\mathrm{c}}=0$, $\Omega_{\mathrm{s}}=0$, $\Omega_x=\Omega_y=\Omega_z=5\Gamma_2$, and we set $\frac{N|\mu_{\mathrm{eg}}|^2}{\varepsilon_0\hbar}=1$ for simplicity. As shown in Fig. 2(a), the probe absorption is distributed in all subspaces under the small probe field detuning ($\Delta_{\mathrm{p}}=2\Gamma_{\mathrm{e}}$). In Fig. 2(b), the probe absorption is mainly situated in the subspaces $(-x,-y,-z)$ and (x,y,z) when the probe field detuning is tuned to $\Delta_{\mathrm{p}}=4\Gamma_{\mathrm{e}}$. Then continue to increase the detuning to $\Delta_{\mathrm{p}}=6\Gamma_{\mathrm{e}}$, we can find in Fig. 2(c) that there only appear two large spheres in the subspaces $(-x,-y,-z)$ and (x,y,z). Furthermore, the volumes of two spheres in the subspaces become smaller when increasing the detuning to an appropriate value ($\Delta_{\mathrm{p}}=8\Gamma_{\mathrm{e}}$), seen from Fig. 2(d). These simulation results illustrate that the value of Δ_{p} has a strong correlation with the absorption of probe field, and the varying of probe detuning alters the absorption of the medium. In this case, a probability of 50% for finding the Rydberg atom in the sub-wavelength region is realized.

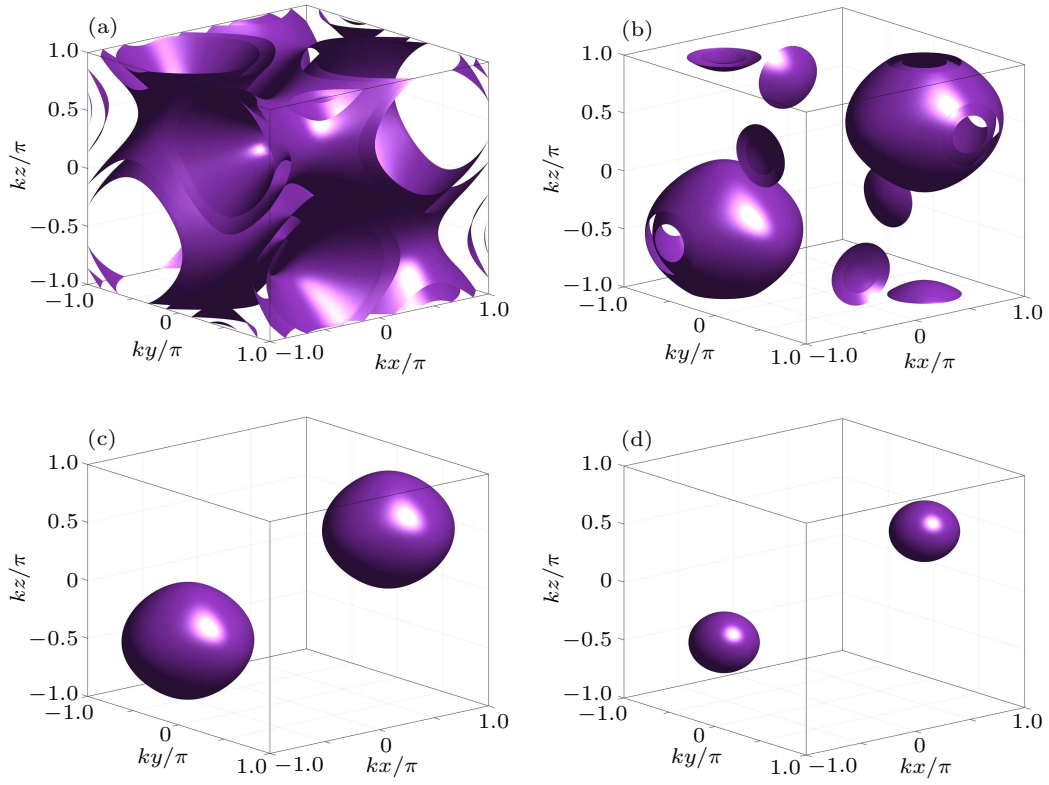

Fig. 2. Isosurfaces of the probe absorption $\mathrm{Im}(\chi)=0.1$ versus positions (kx,ky,kz) for different probe field frequency detunings Δ_{p}. (a) $\Delta_{\mathrm{p}}=2\Gamma_{\mathrm{e}}$; (b) $\Delta_{\mathrm{p}}=4\Gamma_{\mathrm{e}}$; (c) $\Delta_{\mathrm{p}}=6\Gamma_{\mathrm{e}}$; (d) $\Delta_{\mathrm{p}}=8\Gamma_{\mathrm{e}}$. The other parameters are chosen as $\frac{N|\mu_{\mathrm{eg}}|^2}{\varepsilon_0\hbar}=1$, $\Delta=\Delta_{\mathrm{c}}=0$, $\Omega_{\mathrm{s}}=0$, $\Omega_x=\Omega_y=\Omega_z=5\Gamma_2$, $\Gamma_{\mathrm{s}}=0.97\Gamma_{\mathrm{e}}$ and $\Gamma_{\mathrm{s}}=0.05\Gamma_{\mathrm{e}}$. All parameters are in units of Γ_{e}.

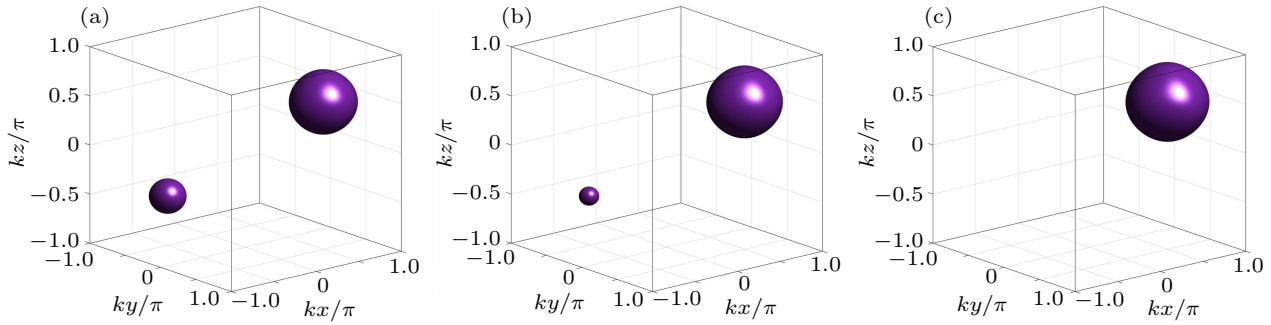

Fig. 3. Isosurfaces of the probe absorption $\mathrm{Im}(\chi) = 0.1$ versus positions (kx, ky, kz) for different traveling-wave fields Rabi frequencies Ω_s. (a) $\Omega_s = 1\Gamma_e$; (b) $\Omega_s = 1.5\Gamma_e$; (c) $\Omega_s = 2\Gamma_e$. The other parameters are the same as Fig. 2(d).

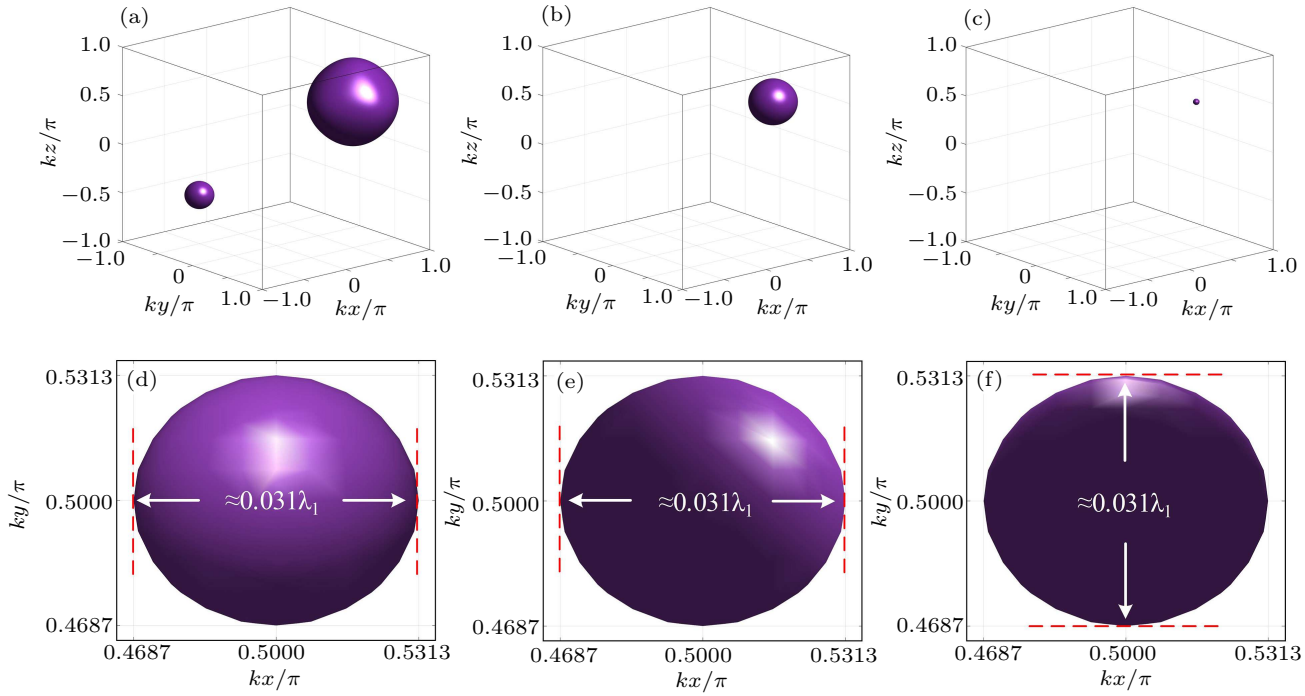

Fig. 4. Isosurfaces of the probe absorption $\mathrm{Im}(\chi) = 0.1$ versus positions (kx, ky, kz) for different combinations of the two frequency detunings (Δ, Δ_c). (a) $(\Delta, \Delta_c) = (3\Gamma_e, 1\Gamma_e)$; (b) $(\Delta, \Delta_c) = (1\Gamma_e, 2\Gamma_e)$; (c) $(\Delta, \Delta_c) = (0.25\Gamma_e, 2.5\Gamma_e)$. (d)–(f) The views of x–y, y–z, and z–x of the minimum localization pattern in Fig. 4(c), respectively. The other parameters are the same as Fig. 3(c).

To locate the Rydberg atom with a higher probability, a traveling-wave field Ω_s is coupled to the transition of $|g\rangle \rightarrow |s\rangle$. Figure 3 investigates the influence of the switching field Rabi frequency Ω_s on the 3D Rydberg atom localization. Here, we choose $\Delta_p = 8\Gamma_e$ for showing clearly the variation trend of the localization patterns. As shown in Fig. 3(a) with $\Omega_s = 1\Gamma_e$, the probe absorption displays a sphere pattern with small diameter in the subspace $(-x, -y, -z)$ and a sphere pattern with large diameter in the subspace (x, y, z). This result indicates that the switching field Ω_s makes the Rydberg atom localization precision different in the two subspaces. In Fig. 3(b), the sphere volume becomes smaller in the subspace $(-x, -y, -z)$ while becomes larger in the subspace (x, y, z) when $\Omega_s = 1.5\Gamma_e$. More interestingly, with further increasing the switching field to $\Omega_s = 2\Gamma_e$, the sphere disappears in the subspace $(-x, -y, -z)$ and there only exists one large sphere in the subspace (x, y, z). This result suggests that we can achieve a 100% probability localization of the Rydberg atom in sub-wavelength region, but the localization precision is low owed to the large volume of the sphere.

In order to improve the precision of the Rydberg atom localization, the influence of two laser frequency detunings (Δ, Δ_c) is studied. Figure 4 illustrates the effect of two frequency detunings (Δ, Δ_c) on the 3D Rydberg atom localization. As we can see from Fig. 4(a), the sphere in the subspace $(-x, -y, -z)$ appears again when $(\Delta, \Delta_c) = (3\Gamma_e, 1\Gamma_e)$. In Fig. 4(b), the sphere in the subspace $(-x, -y, -z)$ disappears and the other in the subspace (x, y, z) becomes smaller than that in Fig. 3(c) when $(\Delta, \Delta_c) = (1\Gamma_e, 2\Gamma_e)$. We find that in the subspace (x, y, z), the sphere becomes smaller with decrease in Δ and increase in Δ_c. The smallest sphere volume is achieved in Fig. 4(c) with $(\Delta, \Delta_c) = (0.25\Gamma_e, 2.5\Gamma_e)$, which indicates that the 3D Rydberg atom localization precision is improved significantly. To further evaluate the precision in determination of the atom position by this scheme, Figs. 4(d)–4(f) show the views of x–y, y–z, and z–x of the localization pat-

tern in Fig. 4(c), respectively. The spatial precision is about $0.031\lambda \times 0.031\lambda \times 0.031\lambda$ under the condition of probe absorption $\mathrm{Im}(\chi) = 0.1$.

Compared with the three-level atom localization schemes,[19,20] this four-level atomic system increases the controllability of the experiment. Thus, the dependence of the localization behavior on the control field Rabi frequency is researched under the above parameters. Figure 5 shows the influence of the control field Rabi frequency Ω_c on the probe absorption. When we increase the control field Rabi frequency Ω_c, the only sphere in the subspace (x, y, z) disappears, which means that the 3D Rydberg atom localization information cannot be obtained. The volume of the sphere gradually becomes larger with decreasing the control field Rabi frequency Ω_c, shown in Figs. 5(a) and 5(b). This suggests that the 3D Rydberg atom localization precision becomes lower with decreasing the control field Ω_c. According to Eq. (3), the density of the Rydberg atoms, N, also affects the precision of localization. We have simulated the influence of the atomic density on the 3D Rydberg atom localization with different values of $\frac{N|\mu_{eg}|^2}{\varepsilon_0\hbar}$,[20] and get the results similar to Fig. 5. That is to say, the detecting precision of 3D Rydberg atom localization is reduced with increasing the cold Rydberg atomic density.

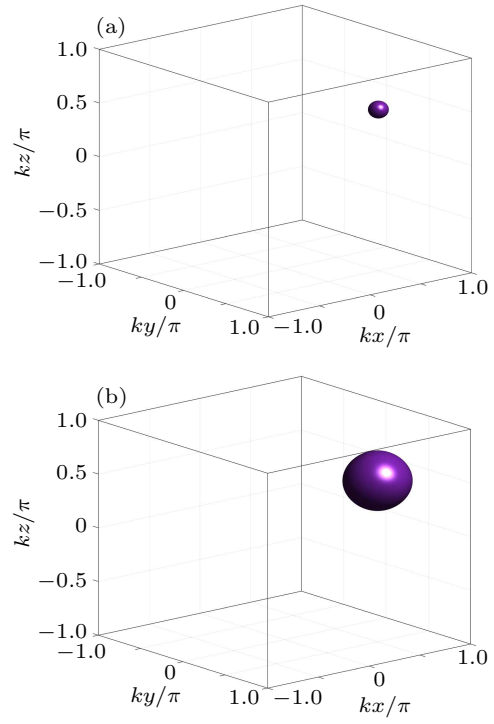

Fig. 5. Isosurfaces of the probe absorption $\mathrm{Im}(\chi) = 0.1$ versus positions (kx, ky, kz) for different Rabi frequencies Ω_c. (a) $\Omega_c = 4\Gamma_e$; (b) $\Omega_c = 2\Gamma_e$. The other parameters are the same as Fig. 4(c).

4. Conclusion

In summary, we have realized a high-precision 3D Rydberg atom localization with the measurement of a weak probe field spatial absorption in a four-level atomic system. The numerical simulation results indicate that the 3D Rydberg atom localization precision can be improved significantly by adjusting the Rabi frequency and detuning of laser fields. More importantly, we realize a 100% localization probability of the Rydberg atom in a specific position, and the spatial precision is about $0.031\lambda \times 0.031\lambda \times 0.031\lambda$ with optimal parameters. By taking cold ^{85}Rb atoms as the candidate to implement, this work demonstrates the possibility for 3D atom localization of the Rydberg atom, which further promotes the applications of Rydberg atoms in the areas of quantum information and many-body physics.

References

[1] Gallagher T F 1994 *Rydberg Atoms* (Cambridge: Cambridge University Press)

[2] Spencer W P, Vaidyanathan A G, Kleppner D and Ducas T W 1981 *Phys. Rev. A* **24** 2513

[3] Ponomarenko D V and Shestakov A F 1993 *Chem. Phys. Lett.* **210** 269

[4] Urban E, Johnson T A, Henage T, Isenhower L, Yavuz D D, Walker T G and Saffman M 2019 *Nat. Phys.* **5** 110

[5] Killian T C, Lim M J, Kulin S, Dumke R, Bergeson S D and Rolston S L 2001 *Phys. Rev. Lett.* **86** 3759

[6] Honer J, Weimer H, Pfau T and Büchler H P 2010 *Phys. Rev. Lett.* **105** 160404

[7] Saffman M, Walker T G and Mølmer K 2010 *Rev. Mod. Phys.* **82** 2313

[8] Müller M, Lesanovsky I, Weimer H, Büchler H P and Zoller P 2009 *Phys. Rev. Lett.* **102** 170502

[9] Sedlacek J A, Schwettmann A, Kübler H, Löw R, Pfau T and Shaffer J P 2012 *Nat. Phys.* **8** 819

[10] Phillips W D 1998 *Rev. Mod. Phys.* **70** 721

[11] Johnson K S, Thywissen J H, Dekker W H, Berggren K K, Chu A P, Younkin R and Prentiss M 1998 *Science* **280** 1583

[12] Yuan J, Wu C, Wang L, Chen G and Jia S 2019 *Opt. Lett.* **44** 4123

[13] Gorshkov A V, Jiang L, Greiner M, Zoller P and Lukin M D 2008 *Phys. Rev. Lett.* **100** 093005

[14] Collins G P 1996 *Phys. Today* **49** 18

[15] Qamar S, Zhu S Y and Zubairy M S 2000 *Phys. Rev. A* **61** 063806

[16] Sahrai M, Tajalli H, Kapale K T and Zubairy M S 2005 *Phys. Rev. A* **72** 013820

[17] Ding C, Li J, Zhan Z and Yang X 2011 *Phys. Rev. A* **83** 922

[18] Wang F and J Xu 2016 *Chin. Phys. B* **25** 104201

[19] Zhu Z, Chen A, Liu S and Yang W 2016 *Phys. Lett. A* **380** 3956

[20] Wang Z, Cao D and Yu B 2016 *Appl. Opt.* **55** 3582

[21] Song F, Chen J, Wang Z and Yu B 2018 *Front. Phys.* **13** 134208

[22] Hong Y, Wang Z and Yu B 2019 *J. Opt. Soc. Am. B* **36** 746

[23] Zhang D, Yu R, Sun Z, Ding C and Zubairy M S 2019 *J. Phys. B: At. Mol. Opt. Phys.* **52** 035502

[24] Luo M, Liu W, Cai D and Gao S 2020 *Chin. Phys. B* **29** 124205

[25] Rahmatullah, Ziauddin, Chuang Y, Lee R K and Qamar S 2018 *J. Opt. Soc. Am. B* **35** 2588

[26] Yuan J, Dong S, Wu C, Wang L, Xiao L and Jia S 2020 *Opt. Express* **28** 23820

[27] Hamedi H R, Sahrai M, Khoshsima H and Juzeliūnas G 2017 *J. Opt. Soc. Am. B* **34** 1923

[28] Scully M and Zubairy M 1997 *Quantum Optics* (Cambridge: Cambridge University Press)